Published in final edited form as:
Biomaterials. 2011 January ; 32(2): 639–651. doi:10.1016/j.biomaterials.2010.08.115.

Multilayered silk scaffolds for meniscus tissue engineering

Biman B. Mandal, **Sang-Hyug Park**, **Eun Seok Gil**, and **David L. Kaplan**
Department of Biomedical Engineering, Tufts University, 4 Colby St. Medford, Massachusetts 02155 USA Fax: (617) 627-3231

David L. Kaplan: David.Kaplan@tufts.edu

Abstract

Removal of injured/damaged meniscus, a vital fibrocartilaginous load-bearing tissue, impairs normal knee function and predisposes patients to osteoarthritis. Meniscus tissue engineering solution is one option to improve outcomes and relieve pain. In an attempt to fabricate knee meniscus grafts three layered wedge shaped silk meniscal scaffold system was engineered to mimic native meniscus architecture. The scaffolds were seeded with human fibroblasts (outside) and chondrocytes (inside) in a spatial separated mode similar to native tissue, in order to generate meniscus-like tissue *in vitro*. In chondrogenic culture in the presence of TGF-b3, cell seeded constructs increased in cellularity and extracellular matrix (ECM) content. Histology and Immunohistochemistry confirmed maintenance of chondrocytic phenotype with higher levels of sulphated glycosaminoglycans (sGAG) and collagen types I and II. Improved scaffold mechanical properties along with ECM alignment with time in culture suggest this multiporous silk construct as a useful micro-patterned template for directed tissue growth with respect to form and function of meniscus-like tissue.

Keywords

Silk; Meniscus; Cartilage; Tissue engineering; Biomaterials

1. Introduction

Tissue engineering applies methods from materials engineering and life sciences to generate artificial constructs for regeneration of new tissues [1]. Meniscus tissue engineering is one such specialized area in need of artificial meniscal grafts mimicking native articular tissue for surgical repairs [2,3]. In Europe alone over 400,000 surgical cases involving the meniscus are performed annually, and over 1 million similar cases are treated in the United States [4]. The current therapeutic strategy for meniscus tears is either partial or subtotal meniscectomy, with only a small percentage of these damaged tissues successfully repaired, with osteoarthritis of the knee a predictable outcome nonetheless [5,6].

A functional intact meniscus is critical for the homeostasis of the knee joint, performing complex knee joint functions for biomechanics in load bearing, load transmission, shock absorption, joint stability and joint lubrication. However, due to lack of vasculature, the human meniscus has poor healing potential. Blood vessels are present only in the outer 10–

Correspondence to: David L. Kaplan, David.Kaplan@tufts.edu.

30% of the meniscal body, where successful tissue repairs occur with a high success rate [6,7]. In contrast, the majority of meniscal tears are in the inner avascular zone where there is a lack of healing and hence needs to be removed and or repaired [8]. Removal and or damage of this anatomical structure lead to degenerative changes of the articular cartilage, osteoarthritis [5,6]. It has been estimated that cartilage volume loss after meniscectomy is 4% per year and is more pronounced in the lateral compartment when compared to medial compartment [9].

To this problem, meniscus allo/autograft transplantation represents a potential solution to substitute for lost meniscal tissue to prevent cartilage degeneration, relieve pain and to improve function. The strategies considered include the delivery of cells to the defect site for repair, including chondrocytes, fibrochondrocytes and stem cells [10–12]. Another strategy is the direct replacement of defective tissue, in part or whole, using natural or synthetic biomaterial scaffolds, including collagen-based grafts, subintestinal submucusa, cell free hydrogels, degradable porous foams, and macro- and microporous polymeric meshes [7,13–17]. Some of these biomaterials have been used for cartilage tissue engineering, including poly-glycolic acid (PGA), poly-L-lactic acid (PLA), copolymers of poly-lactic-co-glycolic acid (PLGA) and alginate [18–21]. However, these materials have intrinsic limitations, including inflammation *in vivo* in the case of the polyesters and rapid degradation and high swelling in the case of collagen, which can limit their use [22–25]. In terms of meniscus shape, a PGA spun matrix was used in a rabbit model but failed to recapitulate the complex internal meniscus architecture [3]. Additional efforts have focused on mimicking the native mesh-like meniscus architecture using cell alignment on biodegradable electrospun fibers for enhanced biomechanics [2,26]. Many of the above studies employed *in vivo* animal models to show chondroprotection by the implants but with a low success rate due to the failure to mimic the complex internal architecture and biomechanics of the native meniscus.

To our understanding, in order to develop a successful tissue engineered meniscus, mimicking its complex internal architecture is most important. In this regard, none of the approaches previously reported have successfully recapitulated the complex native meniscal multiporous and aligned structure as a single meniscus wedge shaped unit to completely and or partially eliminate cartilage degeneration. Thus, in order to mimic the meniscus in a tissue engineered approach, understanding its structural and functional components is important. Meniscuses are wedge-shaped semi-lunar discs attached to the transverse ligaments, the joint capsule, the medial collateral ligament (medially) and the menisco-femoral ligament (laterally) [14,27]. There are three distinct zones in the tissue, the outer finer meshwork, the middle broader mesh-like fibrous structure and the bottom structure with aligned collagen bundles in laminar orientations [28]. These structures contribute to the high tensile and compressive properties of native meniscus [14,28,29]. As a fibrocartilaginous structure, the meniscus has characteristics of both fibrous (outer region) and cartilaginous (inner region) tissues [28,30]. Knee meniscal fibrocartilaginous tissue consists of water (72%), collagens (22%) and glycosaminoglycans (0.8%) [31,32]. Type I collagen accounts for over 90% of the total collagen, while 10% are collagen types II, III and V [27,33]. The peripheral two-thirds of the meniscus consist only of type I collagen, whereas type II collagen comprises a large portion of the fibrillar collagen on the inner side [34]. Proteoglycans are known to contribute 2–3% of meniscus dry weight and are concentrated in the inner cartilaginous region of the meniscus [7,27]. Regarding cell types, at least two cell populations are present within the human meniscus [35]. The fibrochondrocytes are the main cell type within the inner and middle part of the meniscus with rounded or oval shaped structures surrounded by abundant ECM deposition [27,35]. While, the outer one-third of the meniscus is populated by spindle shaped fibroblast-like cells within a dense connective tissue [35].

As a step forward towards meniscus repair and regeneration and embracing the critical role of matrix architecture on functional properties of this challenging tissue, in the present study we investigated the use of a multilayered (tribiology), multiporous silk scaffold system to mimic native meniscus architecture and shape. Fibrous silk protein was chosen as the biopolymer because of its outstanding mechanical properties as well as its biocompatibility, versatile processability into many material formats, and its use in studies of chondrogenesis as well as other tissues [36–40]. Further, the controlled degradability of silk biomaterials allows sufficient time for new tissue integration, maintaining transport and mechanical load during the regeneration process [36,41–43]. In the present study, we hypothesized that cell culture on these highly designed meniscus-like architectures under chondrogenic conditions would result in meniscus-like tissue formation in terms of structure and function.

2. Materials and Methods

2.1 Preparation of silk fibroin solution

A 9 w/v% silk fibroin solution was obtained from *Bombyx mori* silkworm cocoons that were extracted in a 0.02M Na_2CO_3 solution, dissolved in 9.3M LiBr solution and subsequently dialyzed against distilled water [44].

2.2 Meniscus scaffold preparation

3D aqueous-derived silk scaffolds were fabricated into individual layers with different pore sizes and orientations. For the three layers, the first two layers were fabricated according to our previously described salt porogen leaching procedure, while third layer was achieved using freeze drying [44]. Briefly, for salt leaching, two grams of granular NaCl particles (350–400 and 500–600 microns for the first and second layers, respectively) was added per 1 ml of 9 w/v% silk fibroin solution in meniscus shaped polydimethylsiloxane (PDMS) molds at room temperature. Twenty-four hours later the molds were immersed in water to extract the salt from the porous scaffolds over 2 days. Similarly, for the freeze dried third scaffold layer, silk solution was frozen at −80 °C from one direction followed by lyophilization.

2.3 Scanning electron microscopy

Field Emission SEM (FESEM) (Zeiss Ultra55 or Supra55VP, Carl Zeiss AG, Oberkochen, Germany) operating at 6 kV was used for scaffold imaging. Fractured-sections of the scaffolds were obtained in liquid nitrogen using a razor blade. The samples were sputter coated with Pt/Pd before analysis. The scaffold pore sizes were determined by measuring random 25 pores from SEM images using ImageJ 1.40g program (Wayne Rasband, National Institute of Health, USA).

2.4 Cell Expansion

Adult human articular chondrocytes and primary human dermal fibroblast cells were obtained from consenting donors less than 35 years of age (Lonza, Walkersville, MD). The cells were expanded in growth medium containing 90% high glucose Dulbecco's modified Eagle's medium (DMEM), 10% fetal bovine serum (FBS), 0.1 mM nonessential amino acids, 0.29 mg/ml L-glutamate, 1X PSF (100 units/ml penicillin, 100 μg/ml streptomycin, 0.25 μg/ml Fungizone) and 1 ng/ml beta fibroblast growth factor (bFGF, Invitrogen, Carlsbad, CA). Adherent cells formed numerous colonies with time, and were subsequently expanded in the ratio of 1:3. For subsequent experiments, P8 chondrocyte cells were used. Late passage cells were deliberately used as a stringent test for the ability to maintain chondrocyte phenotype and ECM expression.

2.5 Cell seeding on scaffold layers

To produce cell-seeded meniscal equivalents, scaffolds were seeded with human primary fibroblasts at the periphery and human primary chondrocytes at the scaffold center to mimic spatial cell distributions present in native meniscal tissues [7,45]. The scaffolds were cut into discs (8 mm in diameter and 2 mm in thickness) for the study and to manage the cell numbers needed. For cell seeding the scaffolds were sterilized, washed in sterile PBS and conditioned with DMEM overnight before cell seeding. To monitor the response of different meniscus layers in terms of ECM deposition and cell proliferation, both cells types were individually seeded in each scaffold layer. To seed scaffolds, 20 μl aliquots containing 1×10^6 fibroblasts and 0.7×10^6 chondrocytes were loaded onto each scaffold separately. After allowing an additional 1 hour for cell attachment, seeded constructs were cultured in 1 mL of chemically defined medium (DMEM + 10% FBS, 0.1 μM dexamethasone, 50 μg/mL ascorbate 2-phosphate, 40 μg/mL L-proline, 100 μg/mL sodium pyruvate, 1X ITS+ (6.25 μg/ml insulin, 6.25 μg/ml transferrin, 6.25 ng/ml selenous acid), 1.25 mg/ml bovine serum albumin, and 5.35 μg/ml linoleic acid with 10 ng/mL TGF-β3 (R&D systems, Minneapolis, MN) in non-tissue culture treated 12-well plates. This chemically defined medium formulation was used as it has previously been reported to induce as well as maintain chondrogenesis of MSCs and to promote deposition of fibrocartilaginous ECM [26]. Media with supplements was changed every 3 days over a 4 week period.

2.6 Biochemical assays for DNA, GAG and collagen

Scaffold samples (with and without cells) were digested for 16 hrs with papain cocktail (125 μg/ml papain, 5 mM L-cysteine, 100 mM Na_2HPO_4, 5 mM EDTA, pH 6.2) at 60°C for DNA and glycosaminoglycans (GAG) estimation. DNA content was measured using the PicoGreen DNA assay kit as per manufacturer's protocol (Invitrogen, Carlsbad, CA). In brief, the papain digested samples were centrifuged and a 25 μl aliquot of supernatant from each sample was added to a 96 well plate with wells containing 75 μl of 1× TE buffer. A 100 μl aliquot of Quant-iT PicoGreen reagent (1:200 dilution) was added to each well followed by measurement using a fluorimeter with excitation and emission wavelengths of 480 and 528 nm, respectively. A standard curve was generated using lambda phage DNA for quantitation. Total sGAG was estimated using 1, 9-dimethylmethylene blue (DMMB) assay [46]. Individual sample aliquots were mixed with the DMMB reagent and absorbance measured at 525 nm. For estimation of sGAG secreted into the media, spent culture media was stored at −20°C and later assessed for sGAG content using similar protocols. GAG was estimated using a standard curve generated using shark chondroitin sulfate (Sigma, St Luis, MO). For total collagen estimation, the samples were digested in pepsin cocktail (1 mg/ml pepsin, pH 3.0) at 4°C for 48 hrs. The collagen content was measured using a modified Hride Tullberg-Reinert method [47]. In brief, individual digested samples were dried at 37°C in 96 well plates for 24 hrs and reacted with Sirius red dye solution for 1 hr with mild shaking. The dye solution (pH, 3.5) was prepared with Sirius red dissolved in picric acid–saturated solution (1.3%; Sigma, St Luis, MO) to a final concentration of 1 mg/mL. The samples were washed five times with 0.01 N HCL followed by resolving the dye-sample complex using 0.1 N NaOH and recording absorbance at 550 nm. Total collagen was estimated using a standard curve using bovine collagen (Sigma, St Luis, MO). Scaffolds without cells were taken as a blank and values were subtracted in all assays to negate interference. To avoid variations from scaffold sizes and cell numbers, GAG and collagen content were normalized against total scaffold weight and cell numbers, represented by the total DNA content measured by PicoGreen DNA assay kit.

2.7 Histology and immunocytochemistry of constructs

Individual scaffold layers seeded with cells were washed in PBS followed by fixation in 10% neutral buffered formalin for 24 hrs before histological analysis. Samples were

dehydrated through a series of graded ethanol, embedded in paraffin and sectioned at 5 μm thickness. For histological evaluation, sections were deparaffinized, rehydrated through a series of graded ethanols, and stained. Serial sections were stained with hematoxylin and Eosin (H&E) as well as with Safranin-O and Alcian blue for sulfated proteoglycans in the matrix. Similarly, representative constructs were immunostained with monoclonal antibodies against collagen I and II (Abcam, MA). Immunohistochemical sections were deparaffinized, hydrated, and permeabilized. The sections were then incubated for 30 min with 1% bovine serum albumin at 37°C followed by primary antibody for 2 hrs. The sections were washed and incubated with HRP-labeled secondary antibodies (Santa Cruz Biotechnology, Inc. CA) followed by development with diaminobenzidine (DAB) (Vector Laboratories, CA). The sections were counterstained with hematoxylin.

2.8 Confocal microscopy

Fibroblast and chondrocyte cell attachment and spreading on individual *B. mori* silk scaffold layers was assessed using confocal microscopy. For microscopy, each individual scaffold layer was seeded with 1×10^6 and 0.7×10^6 human primary fibroblast and human primary chondrocytes separately, and cultured for 1 and 28 days at 37°C, 5 % CO_2 in medium as above to allow cells to adhere and spread on the matrix. On the day of harvest, the scaffolds were washed three times with PBS (pH 7.4) followed by incubation in 3.7 % formaldehyde in PBS for 10 min. The samples were further washed with PBS and pre-incubated with 1% bovine serum albumin (BSA) for 30 min. The constructs were then permeabilized using 0.1% Triton X-100 for 5 min. Incubation with rhodamine-phalloidin for 20 min at room temperature followed by PBS washing and counterstaining with Hoechst 33342 for 30 min was performed. Images from stained constructs were obtained using a confocal laser scanning microscope (CLSM, Leica SP2 inverted microscope, Mannheim, Germany) equipped with argon (488 nm) and HeNe (534 nm) lasers; two-dimensional multichannel-image processing was performed using IMARIS software (Bitplane AG, Switzerland).

2.9 Mechanical testing

Mechanical characterization of compressive and tensile properties of hydrated scaffolds was determined on an Instron (Norwood, MA) 3366 testing frame equipped with a 0.1 kN load cell. The tests for hydrated scaffolds were carried out in 0.1 (M) PBS at 37°C. The scaffolds were hydrated at least 1 day before tests. To test compressive properties, silk scaffolds were punched out in 4 mm diameter and 3 mm height discs. All tests were accessed with a conventional open-sided (non-confined) configuration and were performed using a displacement control mode at a rate of 5 mm/min. After the compression tests, the compressive stress and strain were graphed based on the measured cross-sectional area and sample height (nominal ~4–5 mm, measured automatically at 0.02N tare load), respectively. The tensile properties of the silk scaffolds (approximately, 20 mm × 5 mm × 1 mm) were measured with a crosshead speed of 0.1% strain s^{-1} and a nominal tare load of 0.02 N applied at 0.3% strain. The dimension of the wet specimens was measured before test. Gauge length was set 14 mm. The yield strength and the compressive modulus were determined from the compressive curves. The tensile strength, modulus, and strain were obtained from the tensile curves. The elastic modulus was calculated based on a linear regression fitting of a small strain section that precedes an identifiable plateau region in both tests. From the compressive curves, the compressive yield strength was determined using an offset-yield approach. A line was drawn parallel to the modulus line, but offset by 0.5% of the initial sample gauge length. The corresponding stress value at which the offset line crossed the stress-strain curve was defined as the compressive yield strength of the scaffold, and is an estimate of the linear elastic and collapse plateau transition point. From the tensile curves, tensile strain (elongation %) was determined as extension normalized to gauge length and ultimate tensile strength was verified as stress where specimen was broken.

2.10 Statistical analysis

All quantitative experiments are run least in triplicates and results are expressed as mean ± standard deviation for n = 4 unless otherwise specified. Statistical analysis of data was performed by one-way analysis of variance (ANOVA). Differences between groups of $p \leq 0.05$ are considered statistically significant and $p \leq 0.01$ as highly significant.

3. Results

3.1 Gross morphology and stacking of engineered silk meniscal constructs

Native meniscus pore heterogeneity was mimicked within silk scaffolds as individual layers (Figure 1). Scanning electron microscopic (SEM) images reveled that the top two layers, fabricated using the salt leaching method, had circular pores in the range of 350–400 and 500–600 microns, respectively. The pores were highly interconnected with inner smaller diameter pores. The bottom third fabricated layer, prepared using the freeze drying method, showed laminar channels with pore widths ranging between 60–80 microns. The scaffolds were shaped like the native meniscus (wedge shaped) and three individual layers can be stacked on top of each other to form a single unit to demonstrate architectural control of the process similar to native meniscus tissue (Figure 1). Figure 2 illustrates how the system can be stacked and integrated into a single unit for graft applications. The concept is to seed cells in each of these silk layers, followed by stacking before use, in a process analogous to our studies of corneal tissue engineering [48].

3.2 Cell attachment and proliferation on individual silk scaffold layers

Confocal microscopy was used to evaluate fibroblast and chondrocyte cell proliferation and attachment in the individual silk meniscus scaffold layers. At day 1, cells appeared clustered and attached onto the walls of the scaffolds. Cell spreading was minimal at day 1 for both the fibroblasts and chondrocytes (Figures 3,4 a,b,c). After day 28 of seeding and culture the cells had filled the voids and spread out actin filaments. In all three meniscal scaffold layers the cells were evenly distributed and confluent (Figures 3,4 d,e,f). PicoGreen DNA assay showed that the chondrocytes proliferated with an increase of ~48, ~64 and ~38% compared to initial cell numbers (day 28 vs day 1) in the case of the 1st, 2nd and 3rd layers, respectively. The fibroblasts showed ~10, ~27 and ~47 % rise in cell numbers, respectively, for the 1–3 layers after 28 days of culture in chondrogenic media (Figure 9a).

3.3 Histology and immunocytochemistry

Histology sections of individual meniscus scaffold layers revealed accumulation of sGAG and collagen with time (day 28 vs day 1) in all three layers. Compared to day 1, samples for day 28 stained deeper for Alician blue, Saffranin O and H&E in all three layers for both cell types (Figures 5,6). For Alician blue, chondrocytes showed intense blue colour suggesting the presence of abundant sGAG. Particularly for the laminar 3rd scaffold layer, the cells stained intense deep blue suggesting mature chondrocyte phenotype (Figures 6B,8). For fibroblasts, the staining was lighter compared to the chondrocytes, but showed positive blue colour on culturing in chondrogenic medium (Figures 5B,8). Similarly, Saffranin O staining confirmed GAG accumulation within scaffold pores in all layers. In the case of Saffranin O staining, faint positive staining of fibroblast cells was observed compared to the intense staining for the chondrocytes (Figure 5C). H&E staining revealed cell attachment and distribution within each scaffold pore/layer suggesting growth and proliferation (Figures 5,6).

Immunocytochemistry staining revealed deposition of collagen I and II within scaffold layers. For both fibroblasts and chondrocytes, collagen I deposition was abundant on day 28 (Figure 7). For collagen II, fibroblasts stained negative when compared to the chondrocytes

(Figure 7). In all scaffold layers, collagen deposition was homogenously distributed with complete filling of pores.

3.4 Biochemical analysis

Histology and immunocytochemistry data was supported by biochemical analysis suggesting the presence of a mature chondrocytic phenotype within the scaffold layers. Both collagen and sGAG increased with time ($p \leq 0.01$) (day 28 vs day 1) (Figures 9,10). Total collagen from the chondrocytes increased ~280, ~266 and ~294 % in the 1^{st} – 3^{rd} scaffold layers, respectively, when compared to day 1 ($p \leq 0.01$) (Figure 9b). This was higher in comparison to the fibroblasts which showed ~47, ~135 and ~164 % increases in total collagen amount in all three layers, respectively, at the same time ($p \leq 0.01$) (Figure 9b). sGAG total (scaffold + media) increased ~209, ~207 and ~330 % for chondrocytes when compared to ~180, ~230 and ~160 %, respectively, for fibroblasts for the 1^{st} – 3^{rd} layers (Figure 10a). However, the total amount of sGAG was comparatively much lower in the fibroblast cells (40–100 μg) as compared to chondrocytes (5–33 μg) after 28 days ($p \leq 0.01$) (Figure 10a). Substantial amounts (~30–40 %) of total sGAG was secreted into the medium while culturing chondrocytes in chondrogenic medium (Figure 10a, d).

The normalized collagen per DNA content increased ~1.5 fold in case of chondrocytes in all layers when compared to a ~0.5 fold for the fibroblasts, though the relative amount was much less for the fibroblasts after day 28 ($p \leq 0.01$) (Figure 9c). Similarly, total sGAG per unit DNA (present in media and deposited in scaffolds) after 28 days of culture, increased ~2.1-fold for the chondrocytes, compared to ~0.3-fold for the fibroblasts ($p \leq 0.01$) (Figure 10b). The secreted GAG was ~30–40% of the total amount of GAG in all three layers (Figure 10a,b). sGAG content was estimated in the chondrogenic medium from each layer and each cell type for 28 days (Figure 10d). Chondrocyte cells reached maximum sGAG production within the first 2 weeks and after this time the amounts were constant. This trend was observed for all three silk meniscus layers.

To assess the effect of different silk layer morphology and matrix features on ECM deposition, total collagen and sGAG were normalized per unit scaffold mass (Figures 9d, 10c). Collagen was independent of the layer morphology with similar collagen deposition at day 28 (Figure 9b,c,d). There was a ~3.5-fold increase in collagen per unit mass of scaffold in the case of the chondrocytes, while a ~1.5 fold increase was found for the fibroblasts (day 28 vs day1) ($p \leq 0.01$) (Figure 9d). However, in the case of the sGAG, an increase in GAG amount (~4.6 fold) was observed for the 3^{rd} layer with laminar morphology seeded with chondrocytes when compared to the first two porous layers (~2.5 fold) after day 28 (Figure 10c).

3.5 Mechanical evaluation of silk meniscus layers

The compressive modulus ranged between 293.78 ± 47.56, 347.58 ± 62.39 and 164.80 ± 14.24 kPa for the 350–400 (1^{st}), 500–600 (2^{nd}) and 60–80 (3^{rd}) scaffold layers, respectively (Table 1). Similarly, compressive strength was 67.23 ± 27.30, 75.62 ± 15.76 and 70.44 ± 09.07 kPa, respectively, for the 1^{st}–3^{rd} scaffold layers. Following tensile testing, both the 1^{st} and 2^{nd} layers were similar in terms of modulus with values in the range of 1.3 MPa with elongation of 40% (Table 1). In comparison, the bottom 3^{rd} layer showed lower values, ~0.26 MPa for tensile modulus, with elongation % much higher at 90% when compared to first two silk layers.

4. Discussion

The success of a cell-based, polymeric tissue engineered meniscus graft relies on its ability to function as a single 3D support matrix mimicking native structure to help graft integration, support cell growth and function to produce tissue-specific ECM [49]. Currently, the only available clinical option for total meniscus replacement is the use of an allograft. However, drawbacks related to the use of allogenic material, including like shape incongruency, potential for disease transmission and limited availability of donor menisci, current meniscus research efforts focus on tissue engineering [2,26,50]. A better understanding of native meniscus tissue morphology and function has helped design culture conditions for meniscus cell growth. However, recapitulating native meniscus tribiology structure and function in an *in vitro* tissue engineered model has been challenging [5,7,14,28,31]. In the present report, we addressed the fabrication of 3D multiporous, multilamellar tissue engineered meniscus, mimicking native meniscus tribiology structure for potential future graft applications.

Primary human cells were selected as the cell source and silk as the biopolymer to assess the concept. The silk was utilized due to its unique material and biological properties as outlined earlier. The heterogeneous tribiology layered structure was used as a guide to fabricate three individual silk scaffold layers of different porosities. The first (top) and second (middle) silk meniscus layer each 2 mm thick represent the heterogeneous pore distribution within a native meniscus having pores of 350–400 and 500–600 microns respectively (Figure 1). The meniscus model of Peterson and Tillmann indicates very fine mesh like pores on the upper layers which are smaller than the top silk layer that we prepared [28]. We began the study based on the hypothesis that with seeded cells grown over time in the presence of growth factors, native ECM will be deposited on top and within the larger pores, forming a fine porous mesh similar to the native tissue (Figures 1,3,4). Further, the fabricated porous silk layers (with larger pores) aid cell migration and form a gradient of ECM mesh sizes by virtue of their different pore sizes, mimicking native tissue architecture over time. The silk layers will contribute high mechanical strength to the construct, resisting *in vivo* shear forces, in future implantations [36]. Our approach contrasts to using a mesh fiber for meniscus engineering [2,26]. Further, the third (bottom) silk layer with laminar channels of 60–80 microns was fabricated to act as a template to allow seeded cells to grow, proliferate and align within the channels (Figure 1). We hypothesized that this will aid aligning deposited collagen and other ECM in a laminar morphology similar to that of the native meniscus, mimicking the aligned collagen bundles contributing to high intrinsic tensile and compressive properties [14,28,29]. From the confocal images it is observed that cells (both fibroblasts and chondrocytes) did form mesh like networks within the pores and aligned structures within the lamina (Figures 3,4). Cells deposited ECM, mainly collagen and GAG, mimicking native tissue morphology and arrangement (mesh and laminar) as further confirmed from histology (Figures 5–7).

Mimicking fibrocartilaginous cellular phenotype was also important towards engineering functional meniscus grafts. To recapitulate native meniscus fibrocartilaginous structure and the spatially separated cellular phenotypes, primary human fibroblasts were seeded as concentric rings on the outside to recreate the vascular fibrous region, while chondrocytes were seeded in the inner concentric zone to represent the avascular cartilage [27,28,30,35]. Fibroblasts and chondrocytes were seeded in each scaffold layer separately and cultured for 28 days to evaluate cell proliferation and ECM production from each layer (Figure 8). From confocal images it was observed that both fibroblasts and chondrocytes became confluent within the scaffold pores and lamina, and had good actin development thoughout (Figures 3,4). The individual silk layers supported cell proliferation with time based on DNA content (Figure 9a). However, fibroblasts showed half the proliferation when compared to the

chondrocytes at day 28, possibly due to differences in initial cell numbers (Figure 9a). Fibroblasts due to their higher initial cell seeding number became confluent early, inhibiting further cell proliferation and resulting in lower DNA values when compared to the chondrocytes. Intense staining of sGAG confirmed maintenance of chondrocytic phenotype and proteoglycan production with time within all individual layered silk structures (inner zones) (Figures 6b,8). The importance of this result is further realized as late passage cells (P8) were used for the experiment, suggesting support of the ability of the matrix to maintain chondrocyte phenotype even for late passage cells. This is similar to the native meniscus, where proteoglycans account for 2–3% of the dry weight and are mainly concentrated in the inner cartilaginous regions of the meniscus (avascular zone) [7,27,51]. Interestingly, the bottom laminar meniscal layer showed more compact mature cartilage phenotype with intense Alician blue and saffranin O staining when compared to the top and middle layers seeded with chondrocytes (Figure 6B). This was possibly due to the close proximity of cells growing between laminar channels (60–80 microns) allowing more subcellular interactions, versus the cells in the top and middle layers separated by pores of few hundred microns (Figures 3,4). The importance of cellular interactions and proximity was also observed based on the cell shape of growing chondrocytes, as they appear more elongated within the larger pores but showed a more compact polygonal morphology with presence of lacunae, similar to mature cells, within the 3rd (bottom) laminar layers (Figure 8). Based on ECM content, the bottom laminar layer produced more sGAG when compared to the other two top layers ($p < 0.01$) (Figure 10a,b,c). We hypothesize that initial cell seeding and substrate morphology impact chondrocyte morphology [2,26,38]. However, based on the intense Alician blue, saffranin O staining and proteoglycan assay results, the chondrocytes maintained their phenotype with time, with sGAG (both deposited and secreted into medium) and collagen production (Figures 5,6,9,10). Interestingly, cultured primary fibroblasts showed positive results for sGAG (Alician blue and Saffranin O), though with low intensity staining, when compared to the chondrocytes, possibly due to the presence of TGF-b in the chondrogenic medium (Figures 5B,8).

Based on the biochemical assays (Figure 9b), increased total collagen further suggests maintenance of a growth microenvironment within the pores and lamina of all the individual silk layers for the cells to grow and secrete ECM similar to native meniscus ($p < 0.01$). Immunostaining showed enhanced production of collagen I and II by cultured chondrocytes at day 28, within the inner (avascular) zone of all silk meniscus layers and analogous to the biochemical composition of native meniscus tissue (Figure 7) [51]. Further, an increase in type I collagen at day 28, along with type II collagen expression, reflects a reversal of any dedifferentiation events that might have occurred due to the higher passage number of the cells used, since P8 cells were used. In comparison, cultured fibroblasts showed positive collagen I and negative collagen II staining in the outer peripheral zone, a feature similar to earlier reported studies on native meniscus [34].

The meniscus is a load bearing structure where mechanical properties are critical in order to withstand *in vivo* stresses. Higher compressive modulus was observed for the second scaffold layer when compared to first layer; while lowest values were observed in case of third layer (Table 1). This was probably a result of thicker pore walls formed in larger scaffold pores when compared to thinner walls within smaller pores. The silk meniscus layers had higher compressive modulii when compared to reported axial (83.4 kPa) and radial (76.1 kPa) compressive moduli for native human medial meniscus [52]. Further, when compared with the human medial meniscus at physiological strain rate, the silk constructs were nearly 1/3 for first and second layer and 1/6 for third layer, when compared to values of 718 and 605 kPa, respectively, for axial and radial compressive moduli [52]. Similarly, considering the anterior (1,048 kPa) and posterior (329 kPa) modulus values for native human meniscus, the silk constructs showed values which were approximately 1/3 for top

two layers and 1/6 for the bottom layer [52]. Further analysis and compared with reported aggregate modulus values at the anterior (160 ± 40 kPa) and posterior (100 ± 30 kPa) of native human meniscus, the silk constructs showed higher values [53]. Regarding tensile properties, we observed values of approximately 1.3 MPa for the first two silk layers with 40% elongation (Table 1). The third bottom layer showed lower values of 260 kPa, but higher elongation of 90% possibly due to the dense laminar morphology with thinner walls. However, the observed values were higher when compared to previous (180–300 kPa) reported results using unseeded PLLA scaffolds [54]. We hypothesize and expect the final values to be enhance to match the native meniscus following cell seeding and ECM deposition on the layers as already observed and reported by others [2,26].

For in vivo applications, graft integration is also an important factor for success. In an effort to combine all three individual cell layers into one functional graft unit, we proposed three individual strategies that could be successfully adopted. We hypothesize that when grown in a composite stack, ECM developed after cell growth and migration within layers would help merge these layers into a single unit over time (Figure 2). However, to aid the process and hold the individual layers together external stitching with silk threads can be considered (Figure 2). Further, in an attempt to quickly assemble these individual pieces into one functional unit, a rivet approach can also be considered, such as by using silk cylindrical pieces pushed into punched holes in the layers (Figure 2). This method will eventually help the entire construct to hold together. The present results are a first step towards a functional human meniscal equivalent, with many issues remaining to be addressed, including: (1) testing the biomechanics of the construct with cells and deposited ECM over time in long term culture, (2) use of other cell types including stem cells and meniscus fibrochondrocytes, and (3) testing the construct *in vivo* for functional outcomes and integration.

5. Conclusions

The results of this study demonstrated the fabrication of a wedge shaped multilamellar/multiporous silk meniscus scaffold with promising mechanical properties and directed tissue growth. Importantly, the individual layers supported robust cell growth with aligned ECM deposition. Fibroblasts and chondrocytes colonized forming spatially separated ECM similar to native tissue, while further optimization will be needed. Biomechanical studies over time may be important for improved mechanics for *in vivo* applications. .

Acknowledgments

We thank the NIH P41 EB002520 (Tissue Engineering Resource Center) for support of this research. Assistance of Sung Jun Kim, East-West Neo Medical Center, Kyung Hee University, Korea in histology is greatly acknowledged.

References

1. Williams D. Benefit and risk in tissue engineering. Materials Today 2004;7:24–29.
2. Baker BM, Nathan AS, Huffman GR, Mauck RL. Tissue engineering with meniscus cells derived from surgical debris. Osteoarthritis Cartilage 2009;17:336–45. [PubMed: 18848784]
3. Kang SW, Son SM, Lee JS, Lee ES, Lee KY, Park SG, et al. Regeneration of whole meniscus using meniscal cells and polymer scaffolds in a rabbit total meniscectomy model. J Biomed Mater Res 2006;77A:659–71.
4. Verdonk PCM, Van Laer MEE, Verdonk R. Meniscus replacement: from allograft to tissue engineering. SportOrthopädie-SportTraumatologie 2008;24:78–82.
5. Fairbank TJ. Knee joint changes after meniscectomy. J Bone Joint Surg Br 1948;30B:664–70. [PubMed: 18894618]

6. Englund M, Roos EM, Lohmander LS. Impact of type of meniscal tear on radiographic and symptomatic knee osteoarthritis: a sixteen-year follow up of meniscectomy with matched controls. Arthritis Rheum 2003;48:2178–87. [PubMed: 12905471]
7. Buma P, Ramrattan NN, van Tienen TG, Veth RPH. Tissue engineering of the meniscus. Biomaterials 2004;25:1523–32. [PubMed: 14697855]
8. Kohn D, Verdonk R, Aagaard H, Seil R, Dienst M. Meniscal substitutes-animal experience. Scand J Med Sci Sports 1999;9:141–45. [PubMed: 10380270]
9. Verdonk R, Kohn D. Harvest and conservation of meniscal allografts. Scand J Med Sci Sports 1999;9:158–9. [PubMed: 10380272]
10. Peretti GM, Gill TJ, Xu JW, Randolph MA, Morse KR, Zaleske DJ. Cell-based therapy for meniscal repair: a large animal study. Am J Sports Med 2004;32:146–58. [PubMed: 14754738]
11. Izuta Y, Ochi M, Adachi N, Deie M, Yamasaki T, Shinomiya R. Meniscal repair using bone marrow derived mesenchymal stem cells: experimental study using green fluorescent protein transgenic rats. Knee 2005;12:217–23. [PubMed: 15911296]
12. Port J, Jackson DW, Lee TQ, Simon TM. Meniscal repair supplemented with exogenous fibrin clot and autogenous cultured marrow cells in the goat model. Am J Sports Med 1996;24:547–55. [PubMed: 8827317]
13. Cook JL, Fox DB, Malaviya P, Tomlinson JL, Kuroki K, Cook CR, et al. Long-term outcome for large meniscal defects treated with small intestinal submucosa in a dog model. Am J Sports Med 2006;34:32–42. [PubMed: 16157845]
14. Sweigart MA, Athanasiou KA. Toward tissue engineering of the knee meniscus. Tissue Eng 2001;7:111–29. [PubMed: 11304448]
15. Kobayashi M, Chang YS, Oka M. A two year in vivo study of polyvinyl alcohol-hydrogel (PVA-H) artificial meniscus. Biomaterials 2005;26:3243–48. [PubMed: 15603819]
16. Kelly BT, Robertson W, Potter HG, Deng XH, Turner AS, Lyman S, et al. Hydrogel meniscal replacement in the sheep knee: preliminary evaluation of chondroprotective effects. Am J Sports Med 2007;35:43–52. [PubMed: 16957008]
17. Heijkants RG, van Calck RV, De Groot JH, Pennings AJ, Schouten AJ, van Tienen TG, et al. Design, synthesis and properties of a degradable polyurethane scaffold for meniscus regeneration. J Mater Sci Mater Med 2004;15:423–27. [PubMed: 15332611]
18. Grande DA, Halberstadt C, Naughton G, Schwartz R, Manji R. Evaluation of matrix scaffolds for tissue engineering of articular cartilage grafts. J Biomed Mater Res 1997;34:211–20. [PubMed: 9029301]
19. Freed LE, Marquis JC, Nohria A, Emmanual J, Mikos AG, Langer R. Neocartilage formation in vitro and in vivo using cells cultured on synthetic biodegradable polymers. J Biomed Mater Res 1993;27:11–23. [PubMed: 8380593]
20. Paige KT, Cima LG, Yaremchuk MJ, Schloo BL, Vacanti JP, Vacanti CA. De novo cartilage generation using calcium alginate chondrocyte constructs. Plast Reconstr Surg 1996;97:168–80. [PubMed: 8532775]
21. Marijnissen WJ, van Osch GJ, Aigner J, van der Veen SW, Hollander AP, Verwoerd-Verhoef HL, et al. Alginate as a chondrocyte-delivery substance in combination with a non-woven scaffold for cartilage tissue engineering. Biomaterials 2002;23:1511–17. [PubMed: 11833491]
22. Cancedda R, Dozin B, Giannoni P, Quarto R. Tissue engineering and cell therapy of cartilage and bone. Matrix Biol 2003;22:81–91. [PubMed: 12714045]
23. Athanasiou KA, Niederauer GG, Agrawal CM. Sterilization, toxicity, biocompatibility and clinical applications of polylactic acid/polyglycolic acid copolymers. Biomaterials 1996;17:93–02. [PubMed: 8624401]
24. Meinel L, Hofmann S, Karageorgiou V, Zichner L, Langer R, Kaplan D, et al. Engineering cartilage-like tissue using human mesenchymal stem cells and silk protein scaffolds. Biotechnol Bioeng 2004;88:379–91. [PubMed: 15486944]
25. Meinel L, Karageorgiou V, Hofmann S, Fajardo R, Snyder B, Li C, et al. Engineering bone-like tissue in vitro using human bone marrow stem cells and silk scaffolds. J Biomed Mater Res 2004;71A:25–34.

26. Baker BM, Mauck RL. The effect of nanofiber alignment on the maturation of engineered meniscus constructs. Biomaterials 2007;28:1967–77. [PubMed: 17250888]
27. McDevitt CA, Webber RJ. The ultrastructure and biochemistry of meniscal cartilage. Clin Orthop 1990;252:8–18. [PubMed: 2406077]
28. Petersen W, Tillmann B. Collagenous fibril texture of the human knee joint menisci. Anat Embryol 1998;197:317–24. [PubMed: 9565324]
29. Tissakht M, Ahmed AM. Tensile stress-strain characteristics of the human meniscal material. J Biomech 1995;28:411–22. [PubMed: 7738050]
30. O'Connor BL. The histological structure of dog knee menisci with comments on its possible significance. Am J Anat 1976;147:407–17. [PubMed: 1036868]
31. Proctor CS, Schmidt MB, Whipple RR, Kelly MA, Mow VC. Material properties of the normal medial bovine meniscus. J Orthop Res 1989;7:771–82. [PubMed: 2677284]
32. Herwig J, Egner E, Buddecke E. Chemical changes of human knee joint menisci in various stages of degeneration. Ann Rheum Dis 1984;43:635–40. [PubMed: 6548109]
33. Eyre DR, Wu JJ. Collagen of fibrocartilage: a distinctive molecular phenotype in bovine meniscus. FEBS Lett 1983;158:265–70. [PubMed: 6688225]
34. Cheung HS. Distribution of type I, II, III and V in the pepsin solubilized collagens in bovine menisci. Connect Tissue Res 1987;16:343–56. [PubMed: 3132349]
35. Ghadially F, Lalonde J, Wedge J. Ultrastructure of normal and torn menisci of the human knee joint. J Anat 1983;136:773–91. [PubMed: 6688412]
36. Altman GH, Diaz F, Jakuba C, Calabro T, Horan RL, Chen J, et al. Silk-based biomaterials. Biomaterials 2003;24:401–16. [PubMed: 12423595]
37. Wang Y, Kim HJ, Vunjak-Novakovic G, Kaplan DL. Stem cell-based tissue engineering with silk biomaterials. Biomaterials 2006;27:6064–82. [PubMed: 16890988]
38. Wang Y, Blasioli DJ, Kim HJ, Kim HS, Kaplan DL. Cartilage tissue engineering with silk scaffolds and human articular chondrocytes. Biomaterials 2006;27:4434–42. [PubMed: 16677707]
39. Meinel L, Hofmann S, Karageorgiou V, Zichner L, Langer R, Kaplan D, et al. Engineering cartilage-like tissue using human mesenchymal stem cells and silk protein scaffolds. Biotechnol Bioeng 2004;88:379–91. [PubMed: 15486944]
40. Meinel L, Karageorgiou V, Hofmann S, Fajardo R, Snyder B, Li C, et al. Engineering bone-like tissue in vitro using human bone marrow stem cells and silk scaffolds. J Biomed Mater Res 2004;71A:25–34.
41. Horan RL, Antle K, Collette AL, Wang Y, Huang J, Moreau JE, et al. In vitro degradation of silk fibroin. Biomaterials 2005;26:3385–93. [PubMed: 15621227]
42. Wang Y, Rudym DD, Walsh A, Abrahamsen L, Kim HJ, Kim HS, et al. In vivo degradation of three-dimensional silk fibroin scaffolds. Biomaterials 2008;29:3415–28. [PubMed: 18502501]
43. Numata K, Cebe P, Kaplan DL. Mechanism of enzymatic degradation of beta-sheet crystals. Biomaterials 2010;31:2926–33. [PubMed: 20044136]
44. Kim UJ, Park J, Kim HJ, Wada M, Kaplan DL. Three-dimensional aqueous-derived biomaterial scaffolds from silk fibroin. Biomaterials 2005;26:2775–85. [PubMed: 15585282]
45. Verdonk PCM, Forsyth RG, Wang J, Almqvist KF, Verdonk R, Veys EM, Verbruggen G. Characterisation of human knee meniscus cell phenotype. OsteoArthritis and Cartilage 2005;13:548–60. [PubMed: 15979007]
46. Whitley CB, Ridnour MD, Draper KA, Dutton CM, Neglia JP. Diagnostic test for mucopolysaccharidosis. I. Direct method for quantifying excessive urinary glycosaminoglycan excretion. Clin Chem 1989;35:374–79. [PubMed: 2493341]
47. Tullberg-Reinert H, Jundt G. In situ measurement of collagen synthesis by human bone cells with a sirius redbased colorimetric microassay: effects of transforming growth factor beta2 and ascorbic acid 2-phosphate. Histochem Cell Biol 1999;112:271–76. [PubMed: 10550611]
48. Lawrence BD, Marchant JK, Pindrus MA, Omenetto FG, Kaplan DL. Silk film biomaterials for cornea tissue engineering. Biomaterials 2009;30:1299–08. [PubMed: 19059642]
49. Temenoff JS, Mikos AG. Review: tissue engineering for regeneration of articular cartilage. Biomaterials 2000;21:431–40. [PubMed: 10674807]

50. Angele P, Johnstone B, Kujat R, Zellner J, Nerlich M, Goldberg V, et al. Stem cell based tissue engineering for meniscus repair. J Biomed Mater Res Part A 2007;85A:445–55.

51. Adams, ME.; Hukins, DWL. The extracellular matrix of the meniscus. In: Mow, VC.; Arnoczky, SP.; Jackson, DW., editors. Knee meniscus: basic and clinical foundations. New York: Raven Press, Ltd; 1992. p. 15-28.

52. Chia HN, Hull ML. Compressive moduli of the human medial meniscus in the axial and radial directions at equilibrium and at a physiological strain rate. J Orthop Res 2008;26:951–56. [PubMed: 18271010]

53. Sweigart MA, Zhu CF, Burt DM, DeHoll PD, Agrawal CM, Clanton TO, et al. Intraspecies and interspecies comparison of the compressive properties of the medial meniscus. Annals of Biomed Eng 2004;32:1569–79.

54. Gunja NJ, Athanasiou KA. Effects of co-culture of meniscal cells and articular chondrocytes on PLLA scaffolds. Biotech Bioeng 2009;103:800–16.

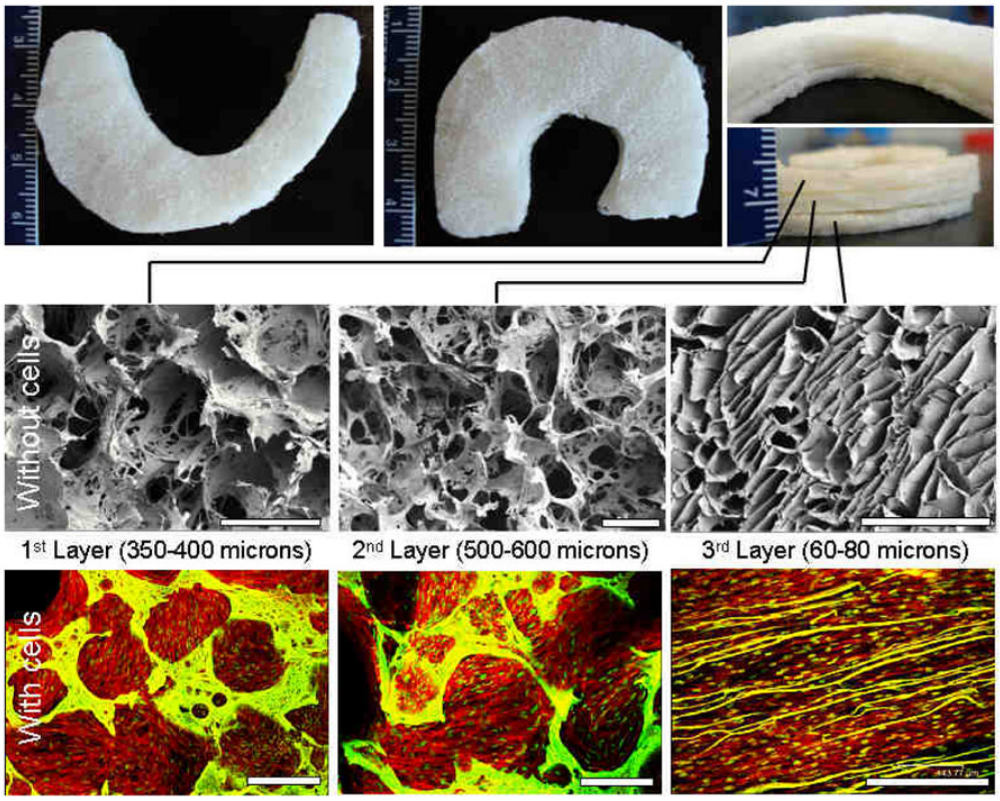

Figure 1.

Regenerated silk scaffolds for functional meniscus engineering. Representative images of fabricated meniscus shaped scaffolds with three stacked layers (Top). SEM images showing porosity and interconnections within pores of individual silk layers without cells (middle) and confocal images of layers with confluent cells (bottom). Scale bar represents 500 microns.

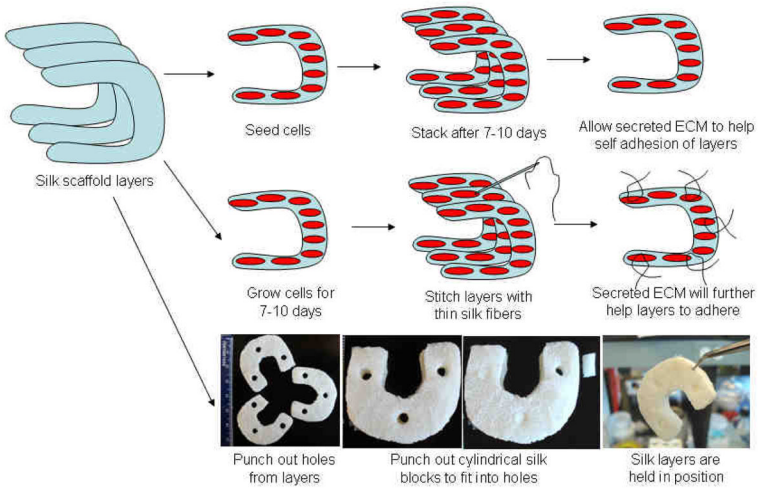

Figure 2.
Possible strategies to be adopted for aligning and integrating individual silk scaffold layers to reconstruct functional meniscus for graft applications.

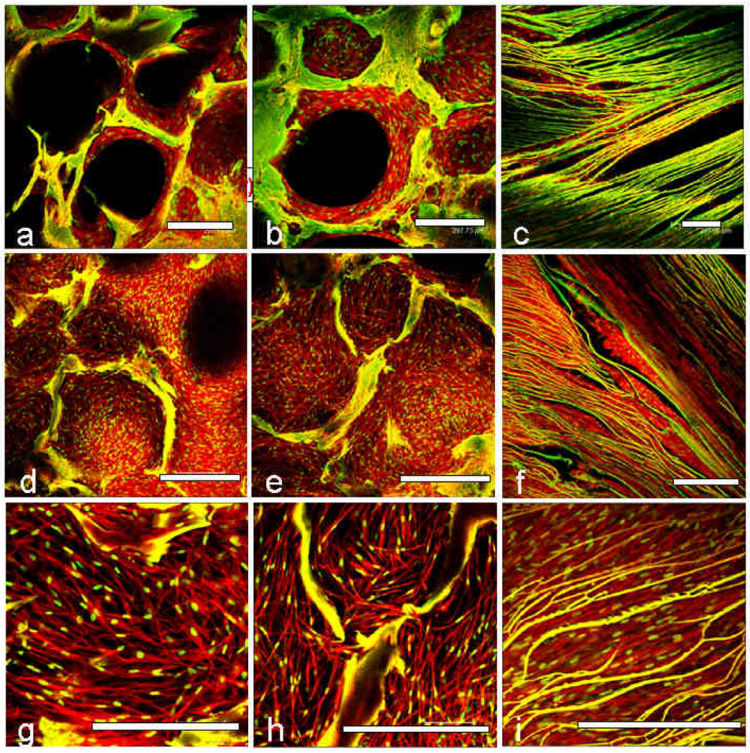

Figure 3.

Confocal laser microscopic images of primary human fibroblast cell attachment, growth and proliferation on individual 3D meniscus silk scaffolds layers in chondrogenic medium. Initial cell attachment on day 1 (a, b, c) and confluent cell covering scaffold pores on day 28 (d, e, f). Magnified images showing cell alignment and spreading within pores and laminas (g, h, i). First/top scaffold layer is represented by (a, d, g); second/middle layer (b, e, h) and third/bottom layer (c, f, i). Scale bar represents 300 microns.

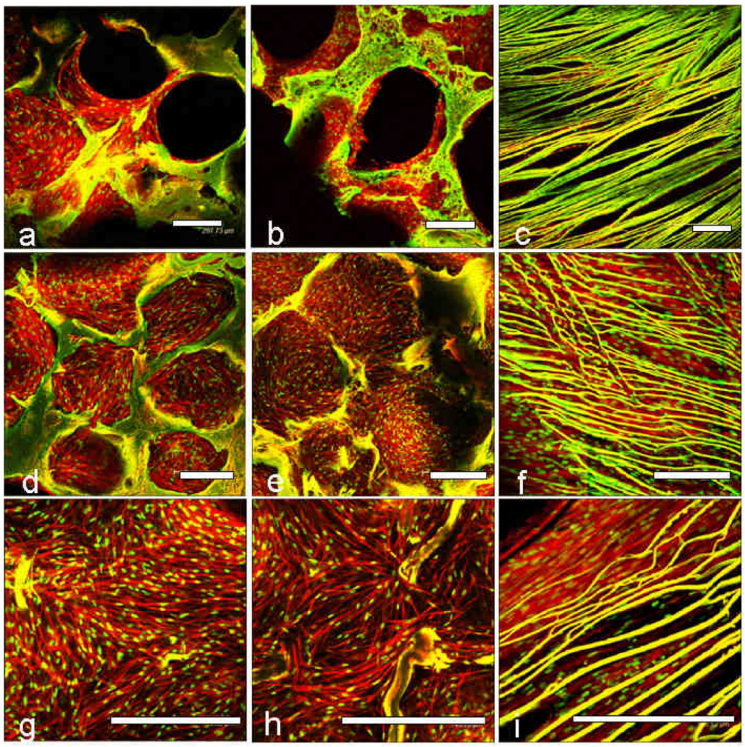

Figure 4.

Confocal laser microscopic images of primary human chondrocyte cell attachment, growth and proliferation on individual 3D meniscus silk scaffolds layers in chondrogenic medium. Initial cell attachment on day 1 (a, b, c) and confluent cell covering scaffold pores on day 28 (d, e, f). Close up images showing cell alignment and spreading within pores and laminas (g, h, i). First/top scaffold layer is represented by (a, d, g); second/middle layer (b, e, h) and third/bottom layer (c, f, i). Scale bar represents 300 microns.

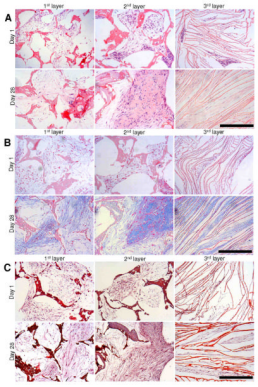

Figure 5.
Histology sections showing primary human fibroblast cell growth and ECM deposition on individual 3D silk meniscus scaffold layers in chondrogenic medium. H and E staining (A); Alician blue staining (B) and Saffranin O staining (C). Scale bar represents 300 microns.

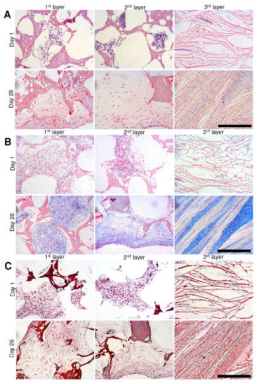

Figure 6.
Histology sections showing primary human chondrocyte cell growth and ECM deposition on individual 3D silk meniscus scaffold layers in chondrogenic medium. H and E staining (A); Alician blue staining (B) and Saffranin O staining (C). Scale bar represents 300 microns.

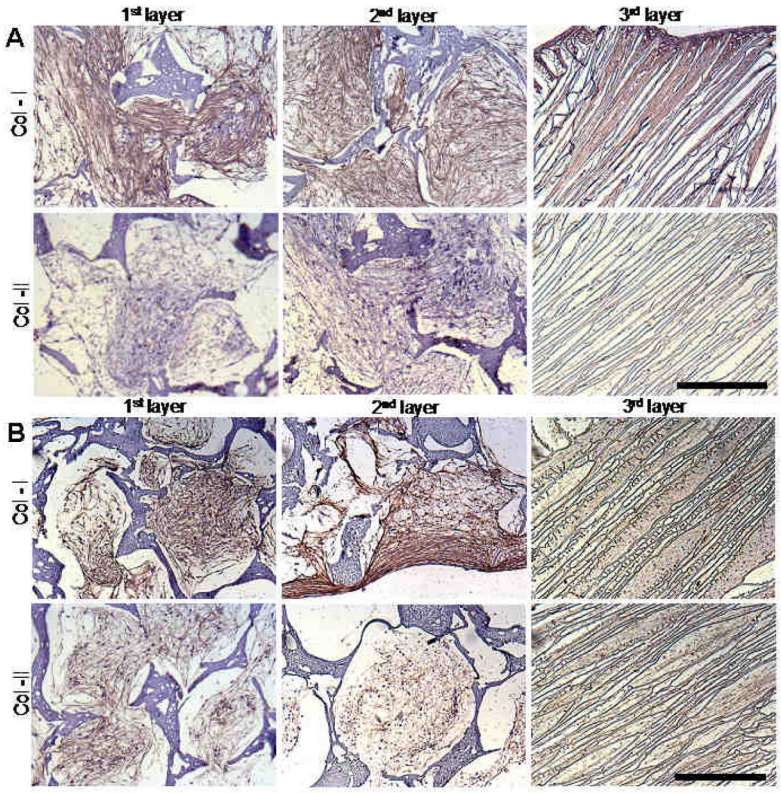

Figure 7.
Silk scaffold histology sections showing immunostaining for collagen I and II. Fibroblast cells (A) and chondrocytes (B) cultured on different scaffold layers cultured for 28 days using chondrogenic medium. Scale bar represents 300 microns.

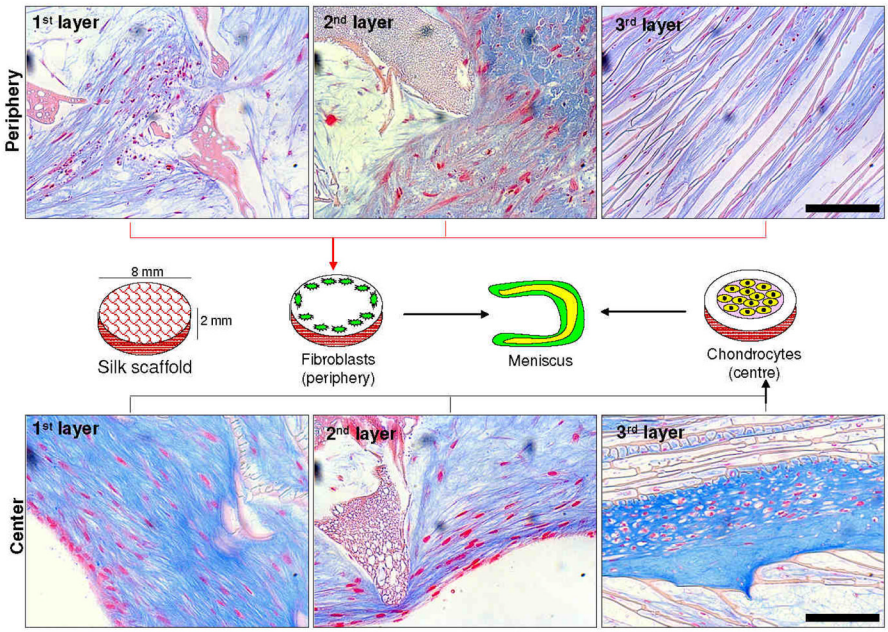

Figure 8.
Schematic representation showing central and peripheral cell seeding on silk scaffold layers mimicking native meniscus tissue cell organization along with histology sections showing matured tissue outcomes. Scale bar represents 100 microns.

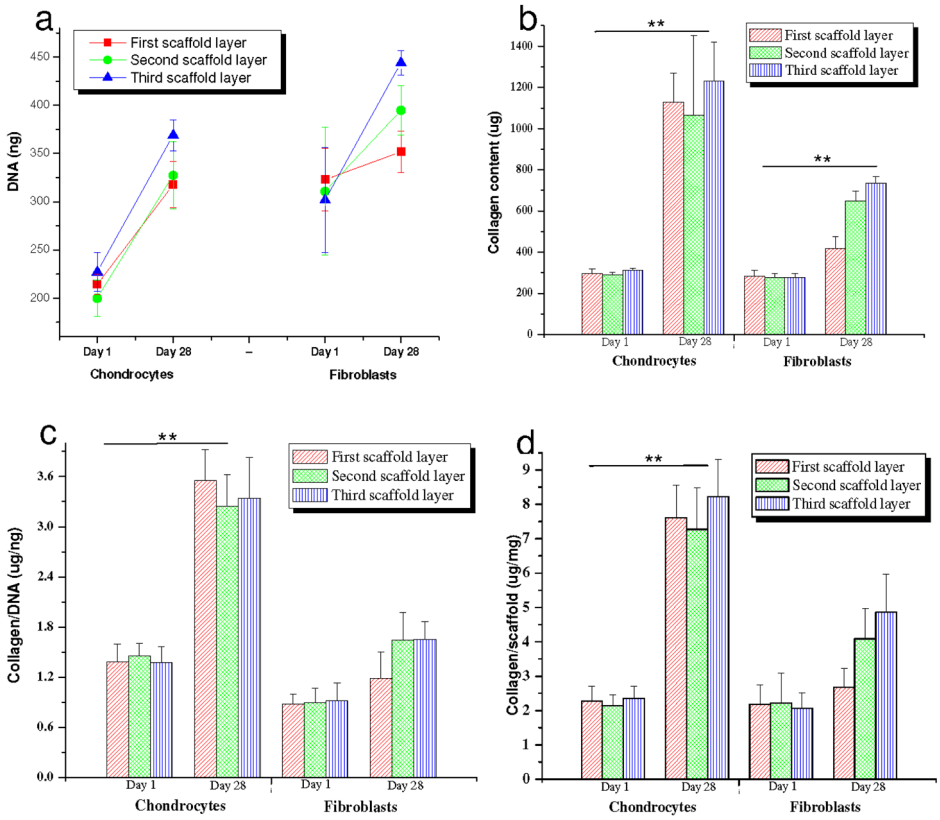

Figure 9.

Biochemical assay results showing (a) DNA content; (b) total collagen; (c) collagen/DNA and (d) Collagen/scaffold estimated in 3 scaffolds layers individually seeded with primary human chondrocytes and fibroblasts in chondrogenic medium after day 1 and 28. Data represents Mean ± standard deviation ($n = 4$, $^{**}p < 0.01$).

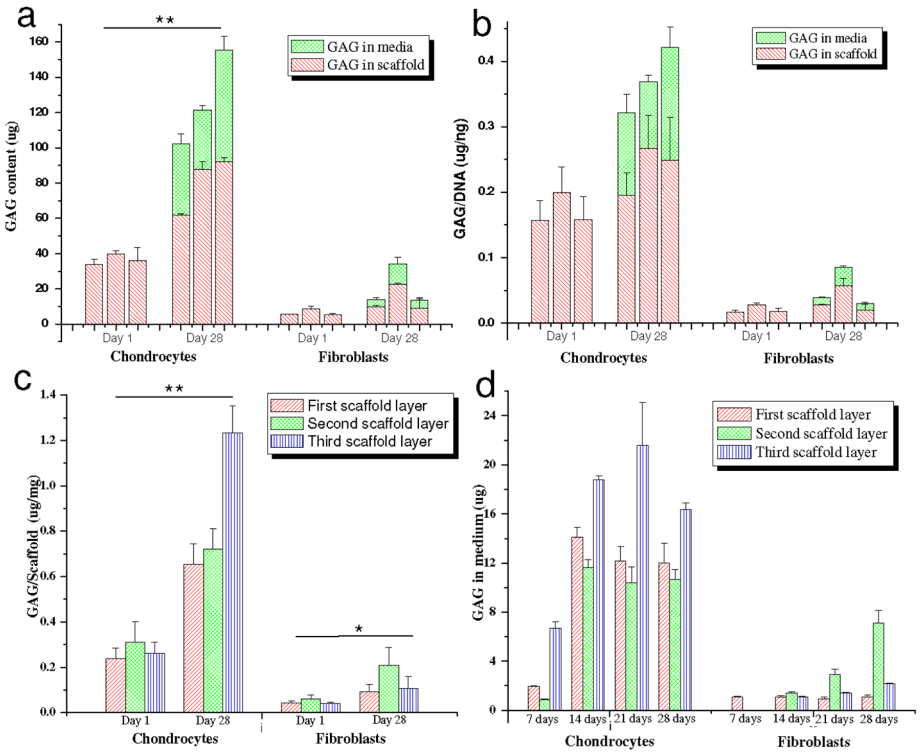

Figure 10.

Biochemical assay results showing (a) total GAG content; (b) GAG/DNA; (c) GAG/scaffold and (d) total GAG in medium, estimated in 3 scaffold layers individually seeded with primary human chondrocytes and fibroblasts in chondrogenic medium after day 1 and 28. Data represents Mean ± standard deviation ($n = 4$, $^{*}p < 0.05$, $^{**}p < 0.01$).

Table 1

Mechanical properties of individual silk scaffold layers.

Silk scaffold layer	Tensile Modulus (MPa)	% Elongation	Compressive Modulus (kPa)	Compressive Strength (kPa)
350–500 (1st layer)	1.30 ± 0.29	42.56 ± 06.91	293.78 ± 47.56	67.23 ± 27.30
500–600 (2nd layer)	1.41 ± 0.41	39.90 ± 07.59	347.58 ± 62.39	75.62 ± 15.76
60–80 (3rd layer)	0.26 ± 0.08	90.62 ± 21.59	164.80 ± 14.24	70.44 ± 09.07